High Energy Laser Driven Electron Acceleration

by

Philip Martin

Supervisor

Dr Gianluca Sarri

A thesis submitted in partial fulfillment for the degree of Integrated Masters in Science (MSci)

in the

School of Mathematics and Physics

March 2015

QUEEN'S UNIVERSITY BELFAST

Abstract

by Philip Martin

An investigation was carried out looking into the process of laser wakefield acceleration of electrons, for the possible application to the generation of multi-MeV γ-rays via nonlinear Thomson scattering. The effects of introducing a gas density gradient just after the accelerating gas cell was tested with the intention of observing an increase in the energy of electrons and an improvement on several other parameters of the beam after acceleration (divergence, relative peak width, and beam pointing). It was found that a density gradient was able to accelerate the electrons to higher energies owing to the longer acceleration lengths, with the final energy being up to 85% larger than the initial energy when shots were averaged out every 5 points. The pointing of the beam relative to the laser axis was also found to stabilise around the zero point after 70 shots, whereas the divergence and relative width of the monoenergetic peaks ($\Delta E/E$) remained relatively constant, with values of $\sim$ 1mrad and $\sim$ 15% the maximum energy respectively. These findings are in line with the hypothesis that stated divergence should not be affected, but energy will be. Further improvements on these results could be obtained with the implementation of hydrodynamic and particle-in-cell simulations of the interactions and experimentation with gas cells of varying density gradients, in order to develop a fully quantitative theory of the laser-gas interaction.

Acknowledgements

I am using this opportunity to express my gratitude to everyone who supported me throughout the course of this MSci project. I am thankful for their aspiring guidance, invaluably constructive criticism and friendly advice during the project work. I am sincerely grateful to them for sharing their expertise on a number of issues related to the project.

I express my warm thanks to my project supervisor Gianluca Sarri, for helping me with any problems I had in the process and for helping to provide me with the knowledge and skills needed to progress on to postgraduate studies.

I would also like to thank Darragh Corvan for helping me with problems I had in implementation of MATLAB codes and for sharing with me his MATLAB script for calculation of electron spectra.

Contents

Chapter 1

Introduction

The invention of lasers with ultrashort pulse durations has opened up new fields of laser-plasma interactions. These pulses can have durations of picoseconds ($10^{-12}s$) and femtoseconds ($10^{-15}s$). This means these pulses can have extremely high powers, on the order of terawatts ($10^{12}W$) and petawatts ($10^{15}W$) with only modest energies of several joules, and focused intensities of over $10^{18}W/cm^2$, with some laser systems such as the HERCULES laser at the University of Michigan have been able to reach intensities as high as $10^{22}W/cm^2$ [1].

When such high intensity lasers interact with matter, the extremely large electric fields present in the light separate electrons from their parent atoms, creating plasmas. Due to these high electric fields, the velocities of the electrons in the plasma can become so large their motion is comparable to the speed of light, making them relativistic and thus opening up the field of relativistic plasma physics, which contains some phenomena of great interest to modern science.

1.1 Chirped Pulse Amplification

When an initial mode-locked oscillator emits a short pulse, on the order of 10's of femtoseconds long with energies of nanojoules (nJ) [2], it is usually necessary to increase the energy of the light via a chain of consecutive amplifiers in order to reach the high powers required for probing relativistic physics. One problem with this however is that the high powers and intensities being dealt with can damage the optical components of the laser. The solution to this is to increase the duration of the pulse by a few orders of magnitude, thus decreasing the power to manageable levels, then decreasing the duration again after the pulse has been sufficiently amplified. This technique of

stretching, amplifying, and compressing the pulse is called chirped pulse amplification (CPA) [3].

Pulse compression and expansion is achieved via the use of pairs of diffraction gratings. The diffraction gratings act to cause different wavelength components of the pulse to travel different distances, thus introducing a time delay in each wavelength component's exit from the gratings and causing the exit pulse to either be shorter or longer than the initial pulse. This results in a phenomenon where the group velocity of the light depends on the frequency and is known as the group velocity dispersion (GVD). The GVD of a system is defined numerically as

$$GVD = \frac{\partial^2 k}{\partial \omega^2} \tag{1.1}$$

Where k and ω is the wavenumber and angular frequency of the radiation respectively. In a stretcher, the short wavelengths are delayed more than the longer ones, and thus as it passes through an arbitrary point in space the stretched pulse will appear to increase in frequency with time. This is known as up-chirping the pulse and occurs when the GVD is positive. When the pulse enters the compressor gratings, which is composed of diffraction gratings with grooves antiparallel to those of the stretcher gratings and thus corresponding to a negative GVD, the longer wavelengths are delayed more so that the pulse is shortened back to its original shape, known as down-chirping the pulse. Below is an example of a simple diffraction grating pair acting as a compressor with negative GVD, showing the longer wavelength, λ_L has to travel further than the shorter wavelength λ_S to reach the same point.

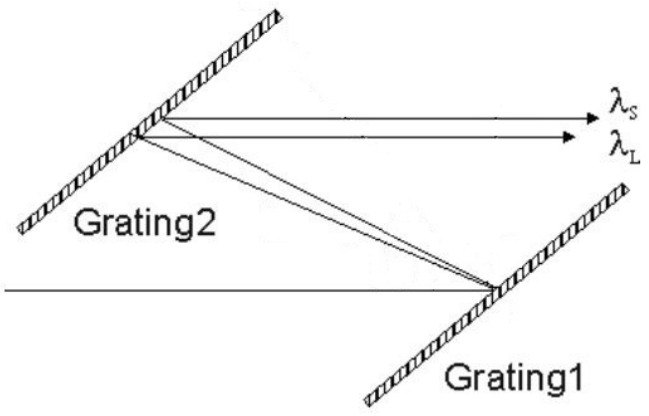

FIGURE 1.1: Grating pair for pulse compression at the end of the amplification chain, showing the different paths taken by long (λ_L) and short (λ_S) wavelengths [4]

The compressor and stretcher are located at opposite ends of the amplification chain. After the pulse is generated from the oscillator, it enters a high gain amplifier known as a front-end amplifier which increases the pulse energy to the mJ level (i.e. a gain of $\sim 10^6$). After this any further amplification would risk damage to the optics in the system, so a stretcher described above is employed to increase the pulse length. After stretching the pulse enters the chain of amplifiers, raising its energy to the joule level. The compressor is then placed after the chain to shorten the pulse back down to tens of femtoseconds.[3]

1.2 Electron Acceleration in Plasmas

An ultrashort laser pulse focused down to micrometer scales can have intensities higher than $10^{18} W/cm^2$. The intensity, I, defined as the time averaged value of the Poynting vector, $\vec{S}$, is related to the electric field of the radiation by [5]

$$I = \langle \vec{S} \rangle = \langle \vec{E} \times \vec{H} \rangle = \frac{\epsilon_0 c}{2} E_0^2 \tag{1.2}$$

Where c is the speed of light in vacuum, $\vec{E}$ is the electric field, $\vec{H}$ is the magnetic field strength defined as $\vec{B} = \mu_0 \vec{H}$, and E_0 is the maximum amplitude of the electric field. Therefore extremely high electric fields are possible (the generated wakefields are typically on the order of hundreds of GV/m to TV/m). When the light interacts with matter, these E fields are high enough to strip atoms of their electrons, forming two fluids of electrons and ions,known as a plasma. Under the right conditions, these high electric fields can then be used to create a wakefield in the plasma, which will accelerate the electrons to extremely high energies (100's of MeV to GeV energies) over distances of a few cm [6]. This is of great interest to modern physics since a conventional linear accelerator can only sustain electric fields of MV/m over accelerating lengths on the order of km for the same electron energy. The reason for this is due to the fact that the solid state components of a linear accelerator will undergo electrical breakdown above a certain threshold, usually on the order of 10MV/m.

1.2.1 Plasma Wakefield Generation

Plasma waves in an intense laser field are generated via the ponderomotive force. The ponderomotive force is a nonlinear force that affects charged particles in an oscillating electric field of very high intensity. It acts to push charged particles away from regions of

high electric field (i.e. high light intensity) to regions of low electric field and is governed by the equation below. [7]

$$F_P = -\frac{e^2}{4m\omega^2}\nabla E^2 \tag{1.3}$$

Where e, m, ω and E are the electric charge of the particle, the mass, angular frequency of the oscillating electric field, and the amplitude of the electric field respectively. When a laser pulse of high enough intensity strikes an underdense plasma (i.e. a plasma of low enough density to allow the wave to propagate through it) the ponderomotive force can drive electrons away from the high intensity regions of the pulse, leaving behind ions and forming a plasma wave in the form of an electron density perturbation oscillating in phase with the laser. Although the ions are also effected by the ponderomotive force, because they are several orders of magnitude heavier than the electrons the force is substantially less. Another consequence of their relatively large mass is the fact that, for short interaction times, their motion can be considered negligible in comparison to electrons, and so are thought of as stationary for the time the laser pulse interacts with the plasma.

In the linear regime, the plasma waves oscillates sinusoidally at the plasma frequency ω_p [8]. The plasma frequency (in rad/s) is defined numerically by

$$\omega_p = \sqrt{\frac{n_e e^2}{m_e \epsilon_0}} \tag{1.4}$$

Where n_e, e, m_e, and ϵ_0 are the electron number density, electron charge, electron mass, and permittivity of free space respectively. The linear regime is defined as when the laser intensity, I, is relatively low, having a value of a_0 that is less than 1. The dimensionless parameter a_0 is the peak quiver momentum of an electron in the electric field of the light oscillating at frequency ω, in units of $m_e c$ [9]. The $(\vec{v} \times \vec{B})$ term in the Lorentz force equation on an electron in the electromagnetic field, $\vec{F} = q(\vec{E} + \vec{v} \times \vec{B})$, can be neglected for nonrelativistic speeds, however for speeds comparable to c, it must be counted and the equation becomes nonlinear. An electron is seen as relativistic when it gains an energy equal to its rest mass energy in half a cycle of the radiation, corresponding to an a_0 of unity. The laser strength parameter a_0 is defined numerically as [10]

$$a_0 = \frac{e}{m_{e0}c}\frac{\lambda}{2\pi c}\sqrt{\frac{2I}{\epsilon_0 c}} = 0.84\sqrt{I[10^{18}W/cm^2] \times (\lambda[\mu m])^2} \tag{1.5}$$

Where λ is the wavelength of the laser light. When $a_0 > 1$, the interaction becomes nonlinear and the group velocity of the plasma wave v_g is approximately equal to the laser pulse group velocity. The frequency of the plasma wave in this regime is lower than the plasma frequency (i.e. the nonlinear plasma waves wavelength λ_{Np} is longer than λ_p) and is given by

$$\omega_{Np} = \frac{2\pi c}{\lambda_p}\left[\left(\frac{2}{\pi}\right)\left(\frac{E_{max}}{E_0} + \frac{E_0}{E_{max}}\right)\right]^{-1}, \frac{E_{max}}{E_0} \gg 1 \tag{1.6}$$

Where E_{max} is the maximum electric field of the light, and E_0 is called the cold nonrelativistic wavebreaking field defined as

$$E_0 = \frac{cm_e\omega_p}{e} \approx 96\sqrt{n_e(cm^{-3})} \tag{1.7}$$

This means that the plasma wavelength increases with increasing electric field amplitude. For a laser pulse with a Gaussian radial profile, as is the case for most lasers, then the plasma wavelength is a function of radius and is shorter towards the edges of the wave, leading to curved wave fronts.

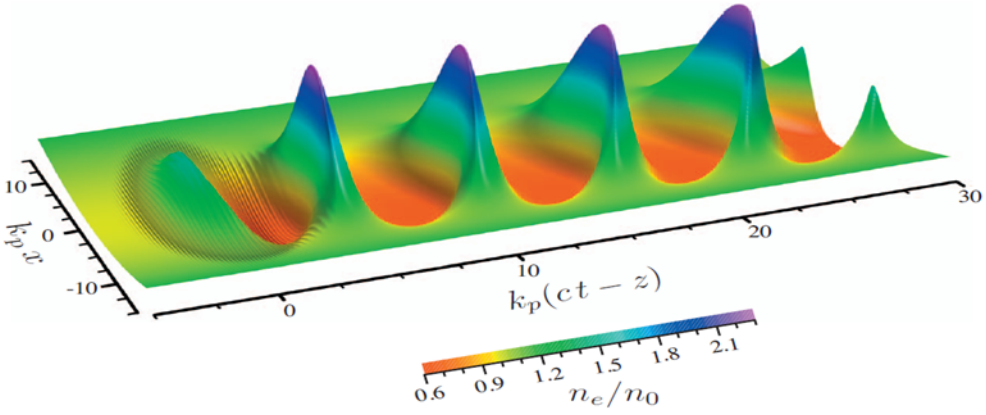

FIGURE 1.2: Plasma density perturbation excited by Gaussian laser pulse travelling to the left with $a_0 = 1.5$ [8]

1.2.2 Laser Wakefield Acceleration and the Blowout Regime

When the right conditions are met, electrons can be trapped in phase with the plasma wave and accelerated to high energies. This process of accelerating electrons using high intensity lasers interacting with a plasma is known as laser wakefield acceleration (LWFA). When the laser pulse is of sufficiently high intensity (i.e. $a_0 > 1$) it can expel almost all electrons from the regions of high electric field, leaving behind ions

forming a positively charged spherical ion cavity which travels just behind and in phase with the laser pulse. This highly nonlinear regime is known as the blowout, cavity, or bubble regime [8, 11]. This cavity can trap a fraction of the expelled electrons behind it, where they are accelerated to highly relativistic velocities from the effect of the space-charge force. The cavity radius is approximately the plasma wavelength, although it can distort and become elliptical with very high intensity pulses. This is due to the larger longitudinal ponderomotive force arising from the steeper intensity gradients associated with such ultrashort pulses.

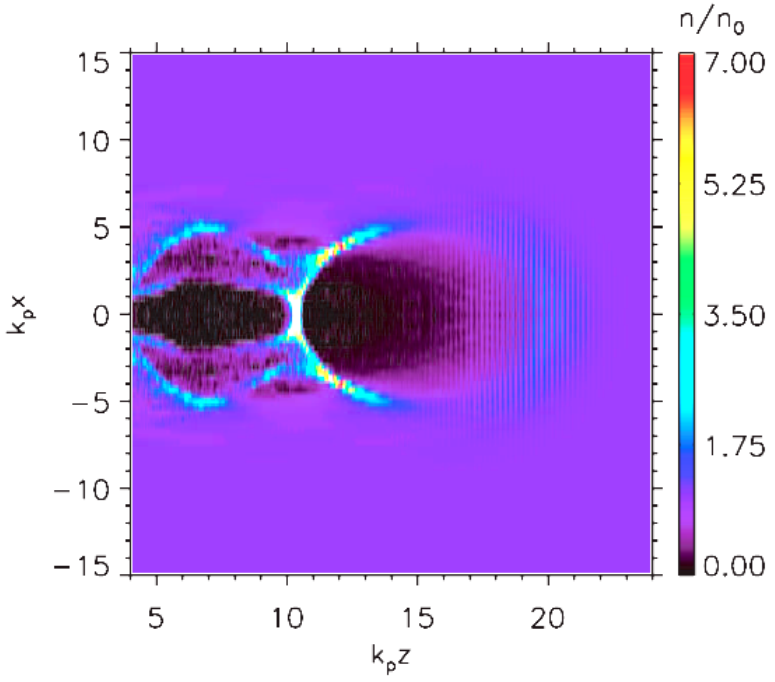

FIGURE 1.3: Electron density map of a plasma wake driven by a laser pulse of $a_0 = 5$ travelling to the right and showing the positively charged cavity (black area) [8]

In order for blowout to occur in the high intensity limit, $a_0 \geq \frac{k_p^2 r_0^2}{4}$ where k_p and r_0 are the wavenumber of the plasma wave and radius of the laser focal spot respectively [11]. It has been observed that the nonlinear blowout regime is more efficient at trapping and accelerating electrons than in the linear regime, and as such is the preferred method for electron acceleration using lasers [12].

1.2.3 Acceleration Limits

Acceleration of the electrons in the plasma wakefield cannot continue indefinitely. There are several processes which limit the distance over which the electron bunch can be accelerated. The main processes are laser diffraction, electron dephasing, and pump depletion. [8]

As the laser propagates through a vacuum, it will naturally undergo diffraction, increasing the laser spot size and decreasing the intensity. This would normally limit the laser plasma interaction distance to a few Rayleigh lengths (defined as $Z_R = \frac{kr_0^2}{2}$), however self-focusing of the laser vastly increases the interaction distance. Self-focusing arises from the optical Kerr effect, which is the phenomenon where the refractive index of an optically nonlinear medium at a point changes with the intensity of the local electric field at that point. Thus, for a beam with a Gaussian intensity profile, the plasma will have a higher refractive index towards the centre of the laser spot, causing the outer edges of the beam to refract in towards the centre, i.e. focusing the laser. Therefore, diffraction is not generally significant for LWFA.

Electron dephasing is essentially a highly relativistic electron bunch outrunning the plasma wave, thus going out of phase with it and decelerating due to the electric field of the ion cavity pulling it back. The distance where the electrons begin to decelerate is called the electron dephasing length, L_d and is described in the nonlinear regime by [12]

$$L_d \simeq \frac{c}{c - v_\phi} r_b \simeq \frac{2}{3} \frac{\omega_0^2}{\omega_p^2} r_b \tag{1.8}$$

Where c is the speed of light, v_ϕ is the phase velocity of the wake, r_b is the radius of the blowout cavity, ω_0 is the frequency of the laser light, and ω_p is the plasma frequency. Below is a graph showing the effects of dephasing on electron energy. As can be seen, the electron energy is a maximum at around 2cm propagation distance, after 2cm they drop off in energy before stabilising at around 2.3cm.

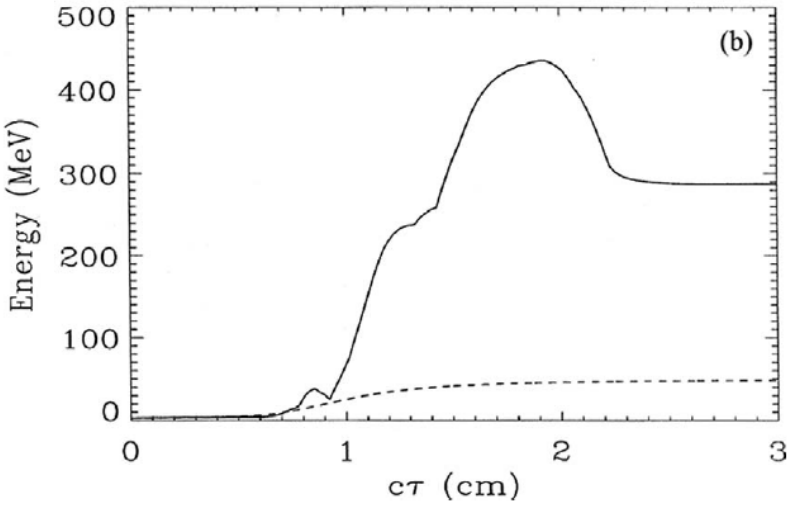

FIGURE 1.4: Peak energy of electrons vs propagation distance [8]

Another mechanism of deceleration is known as pump depletion. As the laser excites the plasma wave, it loses energy to the plasma. The distance over which the laser depletes is called the pump depletion length, given by

$$L_p \simeq \frac{\omega_p^2}{\omega_0^2} c\tau \tag{1.9}$$

Where τ is the time period of the pulse at full width half maximum. In the nonlinear regime, the pump depletion length and dephasing length are roughly the same. The acceleration length is usually set at the dephasing length in order to gave the maximum amount of acceleration possible. The ideal gain in energy of an electron accelerated in a standard LWFA over a length L_{acc} can be calculated from the equation [13]

$$\Delta W = eE_z L_{acc} \tag{1.10}$$

Where E_z is the maximum longitudinal electric field amplitude. Using this equation and converting to practical units, assuming the acceleration is limited by dephasing, the energy gain for the electrons is

$$\Delta W_d(MeV) \simeq \frac{630 I(W/cm^2)}{n(cm^{-3})} \tag{1.11}$$

These equations give the ideal energy gain, and is neglecting various effects, such as instabilities in the plasma or self-focusing of the laser.

When the power is high enough for self-focusing to occur, i.e. in the nonlinear blowout regime, further analysis is needed to refine the above equations. One derivation of the scaling law [14] yielded the refined equation for energy gain

$$\Delta W(MeV) \simeq 0.1 \left(\frac{c\tau}{\lambda}\right) [P(GW)]^{\frac{1}{2}} \tag{1.12}$$

As an example, for a laser pulse of energy 15J and duration 40fs, the energy of the final accelerated electrons comes out as $\Delta W \sim 920 MeV$. In reality, however, the true energy will be lower than this since this is the idealised case.

LWFA continues to improve as time goes on, with the latest results reporting quasimonoenergetic electron beams with energies of up to 4.2GeV using a 0.3PW laser pulse with a duration of around 40fs. [15] These new results prove that LWFA is fast becoming a viable source of high energy electrons and could soon be able to replace conventional linear accelerators for certain applications.

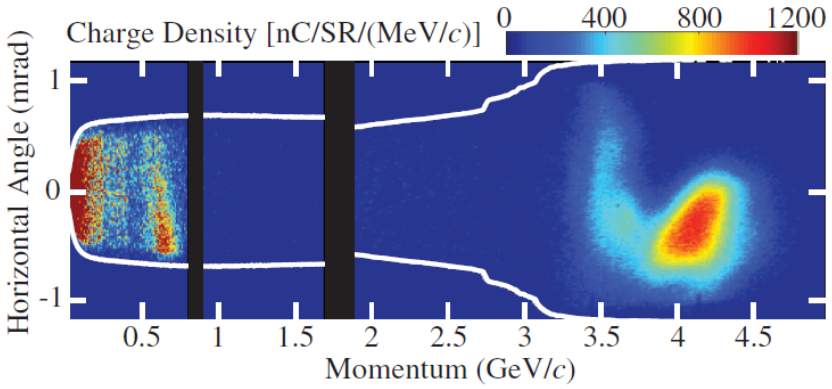

FIGURE 1.5: Energy spectrum obtained by Leemans *et al.* [15] showing the quasi-monoenergetic electron bunch at 4.2GeV, with a tail of lower energy electrons

1.3 X-Ray Generation from Nonlinear Compton Scattering of Relativistic Electrons

One promising application of LWFA electrons is the production of ultrashort high energy, high brilliance, low divergence beams of x-ray and γ-ray radiation produced via nonlinear relativistic Thomson scattering, also referred to as nonlinear Compton scattering [11, 16]. This process involves colliding the electron beam with another counter-propagating ultrashort laser pulse. X-ray energies are reached relatively easily in this regime thanks to two Doppler shifts of the radiation. For the relativistically accelerated electrons with a relativistic factor γ the frequency of the colliding laser pulse in the electron's rest frame is given by

$$\omega' = 2\gamma\omega_0 \tag{1.13}$$

Where ω_0 is the frequency of the radiation in the laboratory frame. This radiation is elastically scattered off the electrons (i.e. scattered at the same outgoing frequency as the incoming frequency). When observed again in the laboratory rest frame, the reflected wave is again Doppler shifted by the same factor as equation 1.13. This gives the final output radiation to be

$$\omega' = 4\gamma^2\omega_0 \tag{1.14}$$

It should be noted that this applies to low intensity laser pulses, i.e. the linear (or undulator) regime of Thomson scattering. When high intensities are applied, nonlinear

Thomson scattering (also called the wiggler regime) dominates and can produce higher order harmonics of this blue shifted radiation so that

$$\omega_r' = n\omega' \tag{1.15}$$

These higher order harmonics arise from the Lorentz force equation which describes electron motion in electromagnetic fields

$$\vec{F} = -e[\vec{E} + (\vec{v} \times \vec{B})] \tag{1.16}$$

When the laser is of a high intensity, the $(\vec{v} \times \vec{B})$ term of the equation, which is normally negligibly small, becomes comparable to the electric field term resulting in a function of electron motion which is nonlinear and relativistic. Thus the motion is no longer harmonic and the emitted radiation consists of a broad spectrum of higher order harmonics. Normally this would cause the spectrum to be upshifted to higher energies as a_0 becomes larger, however the maximum energy is actually lowered with increasing a_0. The reason for this is due to the increase in the electrons effective mass due to the dressing of the electron by the electromagnetic field. This dressed mass is given by [17, 18]

$$m_{eff}^2 = m^2 \left(1 + \frac{a_0^2}{2}\right) \tag{1.17}$$

Leading to an equation for the scattered frequency when dressed mass is taken into account to be [17]

$$\omega' = \frac{4\gamma^2 \omega_0}{1 + \frac{a_0^2}{2}} \tag{1.18}$$

The emitted radiation results from the transverse acceleration of the electrons after being wiggled by the colliding laser pulse. The strength of this wiggling in a conventional solid state magnetic wiggler is determined by the dimensionless strength parameter K, defined as $K = \gamma\psi$ where ψ is the central angle of the emitted radiation with respect to the axis of electron propagation. For a laser pulse, K is represented by a_0.

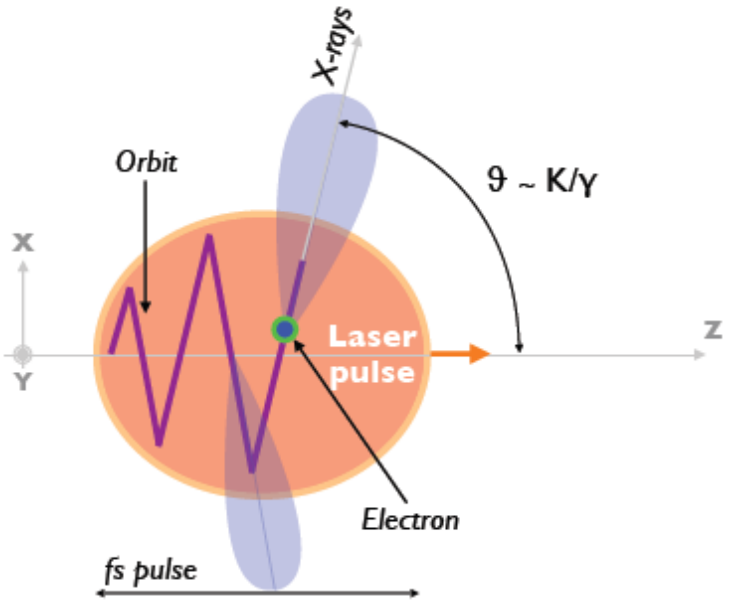

FIGURE 1.6: Nonlinear Thomson scattering, showing electron trajectories in the laser pulse and directions of emitted γ-rays [11]

The system is said to be in the wiggler regime when $a_0 \gg 1$, meaning the electrons undergo a figure 8 motion in their rest frame, which is the origin of higher harmonics. The angular distribution of the radiation is given by the Lorentz factor as $\theta = \frac{1}{\gamma}$. The broadband spectrum of the Thomson scattering ranges up to a critical energy

$$\hbar\omega_c = \frac{3}{2}\gamma^3\hbar\frac{c}{\rho} \tag{1.19}$$

Where ρ is the instantaneous radius of curvature of the electron orbit given by [11]

$$\rho = \frac{\lambda_L}{2\pi}\left(\frac{a_0}{2} + \frac{\sqrt{2}a_0^3}{16}\right) \tag{1.20}$$

Thus, for a highly nonlinear regime where $a_0 \gg 1$ the cutoff energy scales as a_0^3. As can be seen in figure 1.6 the scattered radiation is emitted in two distinct beams, the angular divergence of which are dependent on the Lorentz factor as discussed earlier. This means that the parameter a_0 determines both the energy and divergence of the γ-rays. laser pulses with a higher a_0 will emit more narrowly collimated beams as can be seen in the figure below.

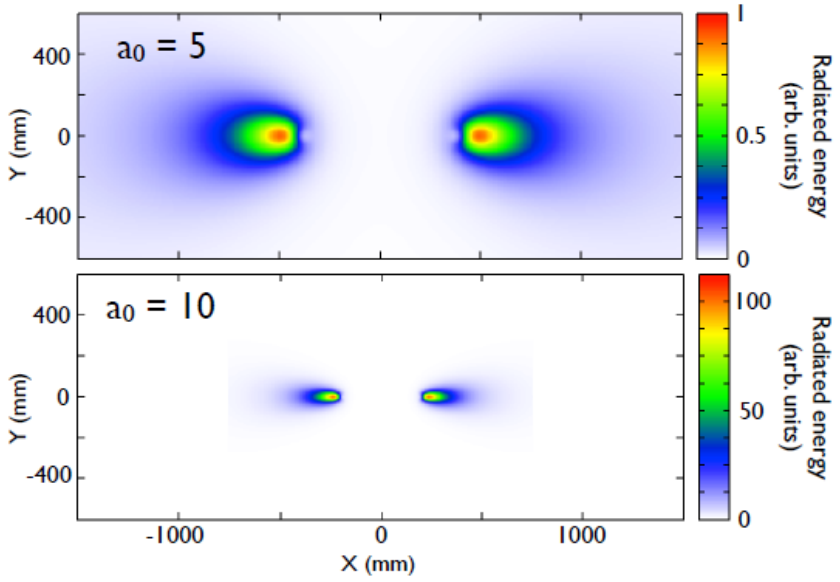

FIGURE 1.7: Spatial distribution of nonlinear Thomson scattering for $a_0 = 5$ and $a_0 = 10$ at a distance of 1m from the source [11]

Nowadays, the radiation produced from nonlinear Thomson scattering can reach very high harmonics, involving energies in the MeV range of highly collimated (milliradian divergence) γ-rays with brilliances up to $1.8 \times 10^{20} photons s^{-1} mm^{-2} mrad^{-2} [0.1\% BW]$ [19].

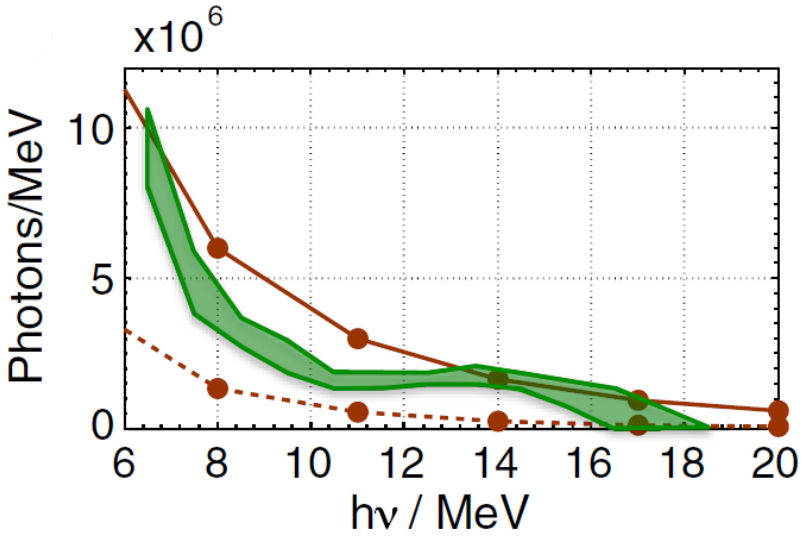

FIGURE 1.8: Typical Thomson scattering x-ray spectrum (green band) obtained by [19] showing energies as high as 18MeV for a laser strength $a_0 = 2$. The solid and dashed lines show the theoretical spectrum obtained with $a_0 = 2$ and $a_0 = 1$ respectively.

These newly achievable energies are highly relevant to cancer treatment [20], opening up the possibility of using this mechanism as a way of delivering radiotherapy to tumours.

This has several advantages over traditional radiation therapy, notably the much higher brilliance associated with this radiation which could be more effective in killing tumour cells due to nonlinear multiphoton interactions with the cell's DNA.

High energy γ-ray beams are also used in research for various applications, and MeV photons could be used to excite giant dipole resonances (GDRs) [21] in large nuclei which can lead to their photofission, a potentially useful method in kick-starting the fission chain reaction for nuclear reactors, or as a probe for active interrogation of nuclei to determine a materials composition from the by-products of photofission, of obvious use in many areas, for example in national security applications [22].

Although this process of Thomson scattering off LWFA electrons has a lot of advantages as listed above, there is still some problems with its implementation. One of these problems is the pointing of the emerging γ-ray beam; that is, the angular deviation from the laser axis. An unstable pointing would be unideal for cancer therapy or active interrogation since the beams need to be precise in order to interact with the tumour/target material. Another problem is the energy spread of electrons. A quasimonoenergetic beam of electrons generally has a tail of low energy electrons following behind it, as shown in figure 1.5. This tail can generate photons which are not of a high enough energy to effectively kill cancer cells in a patient, but could still potentially be ionising, contributing to the damage caused by the radiation while offering little benefit to the patient. In order to refine this so that it is commercially viable, it is useful to eliminate these low energy electrons.

Chapter 2

Experimental Setup

2.1 Experiment

The experiment was performed at the Astra-Gemini laser at the Rutherford Appleton Laboratory. The Astra-Gemini laser is a petawatt class Ti:Sapphire CPA laser system [23]. It is a dual beam system, with both beams originating from the same initial oscillator and amplifier chain, delivering up to 0.5PW beams on target. The beams are of energy 15J and final pulse durations around 45fs, creating focused intensities up to $10^{21} W/cm^2$. Being a broad bandwidth TI:Sapphire (TiS) laser, it operates at a central lasing wavelength of $0.8\mu m$, with a bandwidth of around $0.1\mu m$.

The initial pulse from a TiS oscillator pumped by a frequency doubled neodymium vanadate laser is 12fs long, before being stretched to around 530ps by a pulse stretcher. It is then amplified in a chain of amplifiers before being compressed by a pulse compressor, which is kept in vacuum to prevent breakdown of the air from the high intensities involved. The final output pulse in both beams is 40-45fs long.

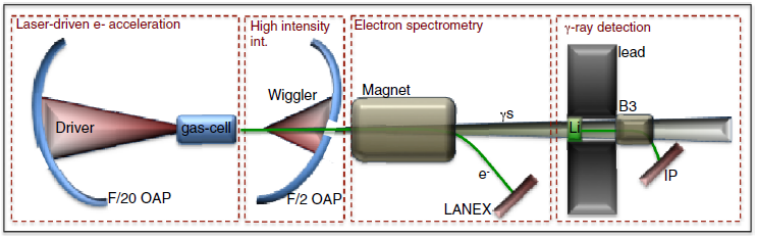

FIGURE 2.1: Sketch of the experimental setup [19] which is described in more detail below

The dual beam design with both beams originating from the same oscillator is ideal for experiments in Thomson scattering of LWFA electrons, since it avoids discrepancies in the synchronisation of the two beams [19]. In the experiment, sketched in figure 2.1, the driver pulse (of duration $\tau \approx 42 \pm 4fs$) was focused using an F/20 off-axis parabolic mirror down to a focal spot of full width half maximum $27 \pm 3\mu m$ which contains around 70% of the laser energy (this corresponds to a focused driver intensity of $I_D \approx 4 \times 10^{19} W/cm^2$ and a laser strength parameter of $a_0 = 2$).

The F number of a parabolic mirror describes how strongly focusing the mirror is. the number N in the term F/N is given by

$$N = \frac{f}{D} \tag{2.1}$$

Where f is the focal length of the mirror, and D is the diameter of the mirror face. Thus, a parabola with an F number of F/20 means that its focal length is 20 times greater than its diameter. An F/2 mirror will be more strongly focusing than an F/20 mirror.

The beam was focused at the entrance of a single stage gas cell 20mm long. The reason a gas cell was chosen instead of a supersonic gas jet which is sometimes used was because the gas contained within a cell is more homogeneous and stationary. Whereas in a gas jet, the high exit speeds of the gas out of the jet can cause density fluctuations, for example from supersonic shock fronts, leading to instabilities in any plasma generated when the laser interacts with it, thus upsetting the acceleration process [24]. The gas cell was filled with a mixture of helium and nitrogen with concentrations of 97% and 3% respectively. The pressure was held at 400mbar initially, and increased gradually to a maximum of around 750mbar. 400mbar pressure corresponds to an electron density in the plasma of $\sim 3 \times 10^{18} cm^{-3}$. Interaction of the laser with the gas created a quasimonoenergetic electron beam via laser wakefield acceleration with energies in the 100s of MeV, and a low energy tail following behind. The divergence of these electron beams were on the order of a few milliradians. The second laser beam was focused using an F/2 parabola (with an F/15 hole in the middle to allow for the photons and electrons to exit the system) to a point 1cm downstream from the exit of the gas cell to act as the wiggler.

Downstream from the F/2 parabola, 65cm from the gas cell, a pair of permanent magnets 15cm long delivering a constant magnetic field of 1T was used to divert the electrons away from the photon beam to a LANEX scintillator screen. This configuration is known as a magnetic spectrometer. The scintillations of the electrons hitting the screen was imaged and the images were use to find the energy spectra of the LWFA electron beam. This is possible because the magnetic field deflects the electrons according to their energy, with higher energy electrons being deflected less than lower energy ones. This means

the electrons horizontal position on the LANEX screen is related to the energy of the particle, and the relative brightness of a point corresponds to the number of electrons at that particular energy. Since the magnetic field acts only on the one plane, the vertical width of the electron beam, d, is unaffected and thus can be measured to derive the divergence of the electron beam by using the formula

$$\theta = \arctan\left(\frac{d}{L}\right) \tag{2.2}$$

Where L is the distance form the LANEX screen to the gas cell, given as 1.3m in this experiment. The position of the electrons on the screen relative to a constant marker could also be used to determine the pointing of the electron beam relative to the drive laser pulse. This LANEX screen can resolve energies between 120MeV and 2GeV. Details of how the energy spectrum can be described mathematically on the screen is discussed later on.

The γ-rays were then spectrally resolved further downstream using a block of lithium, which generated secondary electrons via Compton scattering. The electrons scattered on axis were detected in a similar fashion to the wakefield electrons discussed above, and once their energy spectrum was determined, the γ-ray spectrum was able to be inferred from this with MeV resolution, since the electron spectrum retains the same shape as the incident γ-ray beam [25].

2.2 The Magnetic Spectrometer

The magnetic spectrometer is used to determine the energy spectrum of an electron bunch from measurements of a magnetically deflected electron beams horizontal position and relative brightness when scintillated on a LANEX screen. It can also be used to simply determine the divergence and pointing of the electron beam (on one axis only, that is perpendicular to the axis of deflection or energy spread) as stated above. In this section, the basic mathematics of the magnet spectrometer will be discussed.

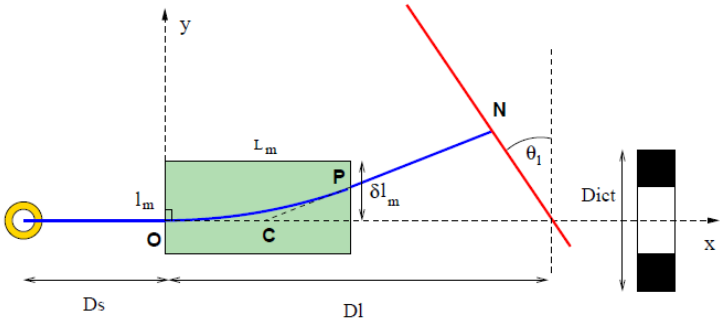

FIGURE 2.2: Diagram showing the basic setup of a magnetic spectrometer [26] with all parameters described in the equations below. The green highlighted area is the region of magnetic field

For an electron of energy E_0 in a uniform magnetic field B, the radius of curvature, R, of the electron trajectory is given by [26]

$$BR = \frac{\sqrt{E_0(E_0 + 2m_e c^2)}}{ec} \tag{2.3}$$

When the electron is relativistic, i.e. $E_0 \gg 2m_e c^2$, this equation can be reduced to

$$BR \simeq \frac{E_0}{ec} \tag{2.4}$$

The electron trajectory can be determined using geometric analysis. The electron describes a circle when in the presence of a magnetic field, and travels in a straight line otherwise. On entering the magnetic field region perpendicular to the magnet surface at the origin O of an arbitrary coordinate system determined by the laser axis of propagation, the electron exits the area at a point P with coordinates governed by

$$(x_P, y_P) = (L_m, R - \sqrt{R^2 - L_m^2}) \tag{2.5}$$

Where L_m is the length of the magnetic field along the x axis. After this point, the electron then traces a straight line to the LANEX screen. If this straight path is traced back, the point C where this tangent intersects the x axis is given by

$$(x_C, y_C) = \left(\frac{x_P^2 + y_P^2}{2x_P}, 0\right) \tag{2.6}$$

Where OC = CP. And finally, the coordinate of the point N on the scintillator screen where the electron hits is given by extrapolating a straight line from the point C

$$(x_N, y_N) = \left(D_l - y_N \tan(\theta_l), \frac{(D_l - x_C)y_P}{x_P - x_C + y_P \tan(\theta_l)} \right) \tag{2.7}$$

Where θ_l is the angle of the scintillator screen with respect to the magnetic field and D_l is the distance from the beginning of the magnetic field to the scintillator screen along the laser axis. From these coordinates, one can work backwards to find R, and thus energy of the electrons, since all other parameters are constant for the experiment.

These equations are reliant on the assumption that the electrons are all perfectly perpendicular to the magnet (i.e. the beam has a divergence of 0). In reality there will be an intrinsic resolution for a certain energy in the spectrometer which is dependent mainly on the divergence of the beam. The resolution of this spectrometer, derived in [26], is given as

$$\frac{\delta E}{E_0} \sim \frac{(D_s + D_l)R\theta_s}{(D_l - L_m/2)L_m} \tag{2.8}$$

As $E_0 \to \infty$ and where D_s and θ_s are the distance from the source to the magnetic field and the angular divergence of the electron beam respectively. If the electron is ultrarelativistic (i.e. $E_0 \gg m_e c^2 \approx 0.5MeV$) then using equation 2.4 the resolution can be rewritten as [25]

$$\frac{\delta E}{E_0} \approx \frac{E(eV)}{cB} \frac{(D_s + D_l)\theta_s}{(D_l - L_m/2)L_m} \tag{2.9}$$

For the parameters of the experiment we performed, $B = 1T$, $D_s = 65cm$, $D_l = 65cm$, $L_m = 15cm$ and $\theta_s \approx 1mrad$. These values gave the following graph of the spectral resolution of the spectrometer for energies between 100MeV and 1GeV.

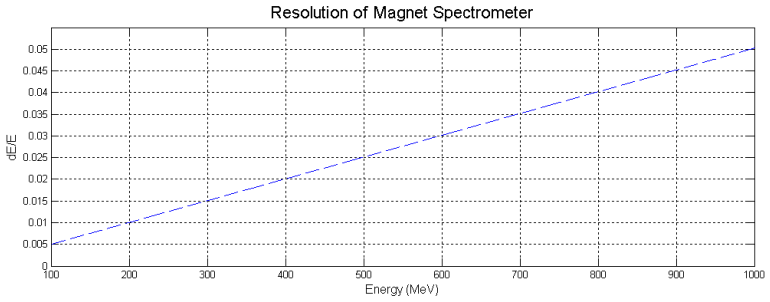

FIGURE 2.3: Resolution of the magnet spectrometer for the parameters discussed above

As can be seen, the energy resolution decreases linearly with the energy, which is to be expected since the faster electrons would have less time to interact with the magnetic field, and would tend to bunch closer together at higher energies as a result. Having a maximum resolution of 5% at 1GeV energies (corresponding to 50MeV resolution) is a very good quality, owing primarily to the extremely low divergences of such electron beams.

Chapter 3

Results and Discussion of Electron Spectra

3.1 Density Gradient Hypothesis

When the experiment was being performed, it was observed that the energies of the electrons appeared to be getting larger, as if the electrons were being accelerated by either a larger electric field, or over a longer acceleration length. Since the laser intensity was kept at a constant value for the entirety of the experiment, the electric field is not larger. It was hypothesised that the electrons were being accelerated over a longer distance than the length of the gas cell. The counter propagating laser that acts as the wiggler is thought to ablate the exit hole of the gas cell. This ablation would cause the hole to get bigger linearly over time as more and more shots were taken. As the hole gets bigger, some of the gas leaks out of the cell, creating a density gradient that decays exponentially over distance from the gas cell, as in the figure below. The density gradient would become more significant as the hole gets bigger, effectively increasing the length of plasma over which the electrons can accelerate, thus increasing their maximum energy.

While longer acceleration lengths with gas cells are ineffective due to electron dephasing as discussed earlier, this is with the assumption that the electron density stays constant over the full length of the acceleration. With a density gradient, the laser pulse and following bubble cavity would actually propagate faster and faster over time due to the decreasing refractive index of the medium. This speeding up of the laser pulse prevents the electrons from outrunning the pulse and dephasing, allowing them to be accelerated over the additional length of the density gradient.

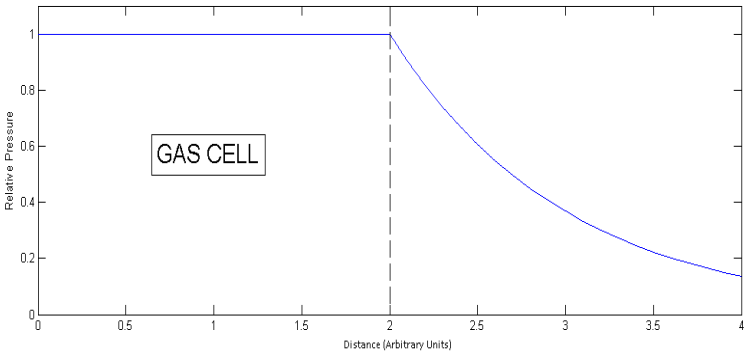

FIGURE 3.1: Example of the exponential decay of gas density after gas cell with a large ablated exit hole. Distances shown here are not necessarily accurate.

While the electrons peak energy would be expected to increase in the presence of such a density gradient, The electron beam divergence and pointing is not expected to change by any significant amount. This is because the beam divergence is determined by the amount of curvature of the plasma wavefronts, as in figures 1.2 and 1.3. The electrons towards the edges of the wavefronts are accelerated by an electric field that has a transverse component as well as a longitudinal component, thanks to the edge of the wave not being perpendicular to the axis of propagation. This transverse component acts to accelerate the electrons at an angle to the laser axis determined by the wavefront curvature and it is this angle which gives rise to the beam divergence. With a density gradient, the wavefronts are not expected to deviate in their degree of curvature when compared to a pristine gas cell with no density gradient. The pointing of the electron beam is also not expected to change over time, since that is also determined within the region of constant density inside the gas cell.

3.2 Results and Discussion

There are 4 parameters of interest in this experiment. These are the electron beam divergence, pointing, central energy of the monoenergetic peak, and the width of the monoenergetic peak (given by $\Delta E/E$). Electron energy spectra could be found by taking an image of the electrons on the scintillator screen, as shown in figure 3.2 below, subtracting the background brightness in imageJ to remove excess noise, and processing the image with a script written in MATLAB which will turn the horizontal distance along the screen, found using a scale present in each picture (determined to be 65 pixels every 10mm), and relative brightness of each point into energy and number of electrons, respectively.

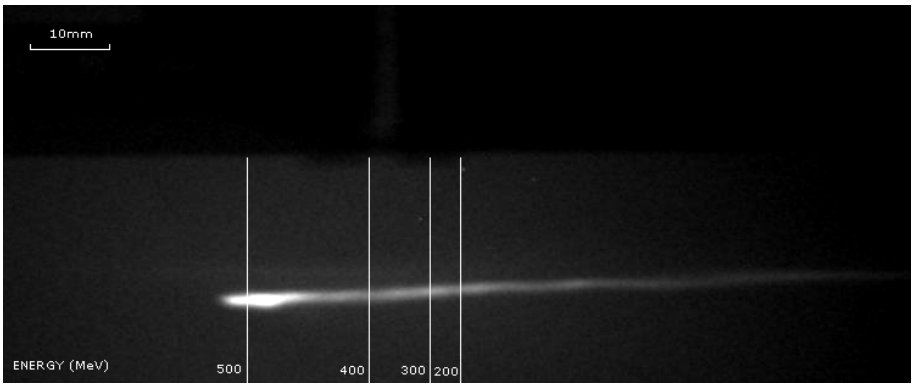

FIGURE 3.2: An example of an electron image taken on the LANEX screen, before background noise subtraction. The horizontal scale represents energy decreasing to the right in units of MeV. The bright monoenergetic peak can be seen at the far right of the streak, with the dimmer low energy tail trailing to the right. The scale at the top of the image is used to determine distances

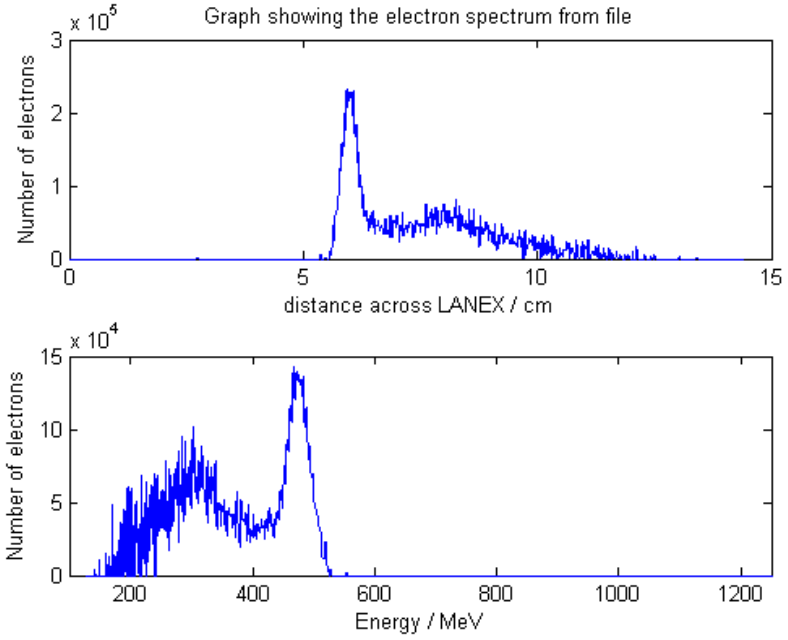

FIGURE 3.3: Electron spectra obtained in MATLAB of the above image. The first graph showing the electron number against the horizontal position on the screen. The second graph shows the electron number against energy

In the electron spectra obtained in figure 3.3, the quasimonoenergetic peak is clearly visible, with the low energy tail following behind. Note that the spectrum is flipped when converted into energy units, since the higher energy electrons are positioned at a lesser distance down the screen than the low energy ones.

3.2.1 Peak Electron Energy

The main point of the hypothesis was that the energy of the electrons' monoenergetic peaks would increase with time. So a plot of peak energy against shot number should show a gradual linear increase. The energy of the midpoint of the peaks were calculated from the graphs plotted of the spectra in MATLAB. These were plotted against the shot number and the graph below was produced.

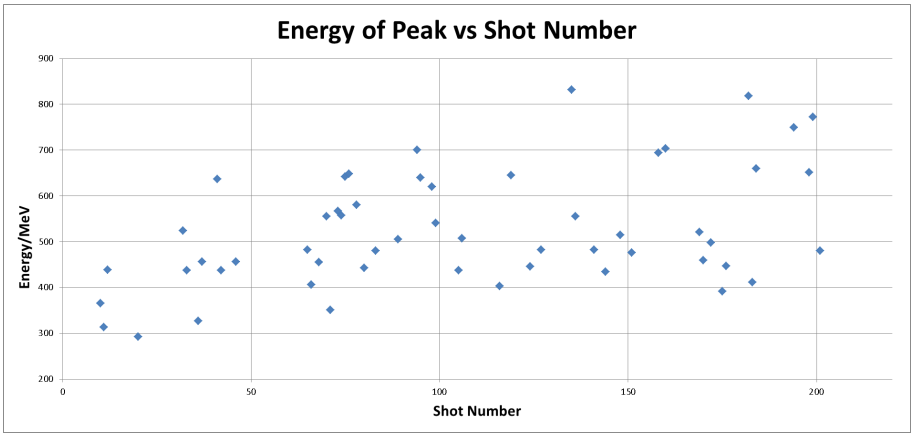

FIGURE 3.4: Energy of the monoenergetic peaks against shot number

It should be noted that shots after shot 213 were not counted since the gas cell was changed after then. As can be seen in the figure, there is a great deal of shot-to-shot variation, and while the shots may appear to increase in energy on average over time, that assumption cannot be made. To further test the hypothesis, the average shot energy was taken for every 5 consecutive shots, and this was plotted against the average shot number for those points. Error bars were fitted, and defined as the standard deviation of each point making up the average.

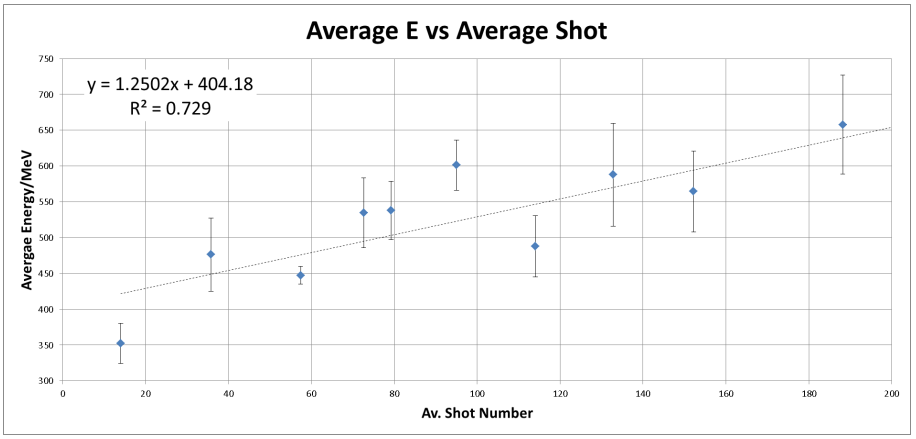

FIGURE 3.5: Average energy every 5 shots average shot number, with error bars and trendline fitted to the data

Here the upward trend is much more clear, with a calculated trendline equation $y = 1.25x + 404$ with an R^2 of 0.73. The data was determined to be statistically significant if the linear trendline plotted had a difference between its lowest and highest points larger than the standard deviation of the points making up the graph. The rise of the trendline was calculated as ∼250, and the standard deviation of the points was calculated to be σ ∼88. Thus, the data is deemed to be statistically significant, and the average electron peak energy rises as the number of shots increase, with the final point having a value of average energy 85% larger than the first point. Although the individual shot energies can vary by relatively large amounts, this verifies the idea of hole ablation and density gradients help to increase the final electron energy. In the future, this density gradient could be utilised in achieving higher electron energies, although further research would be needed in this area, in particular simulations of exactly how the gas leaks out of the cell.

3.2.2 Electron Peak Width

The degree to which a peak is monoenergetic is given by the relation $\frac{\Delta E}{E}$ where ΔE is the full width half maximum of the peak. To calculate the FWHM of each peak, a Gaussian curve line of best fit was plotted around the peaks points, and from this a script was written in MATLAB to calculate the FWHM of the curve. $\frac{\Delta E}{E}$ was then plotted against shot number to test whether a the presence of a density gradient affects the peak widths, as well as their energies.

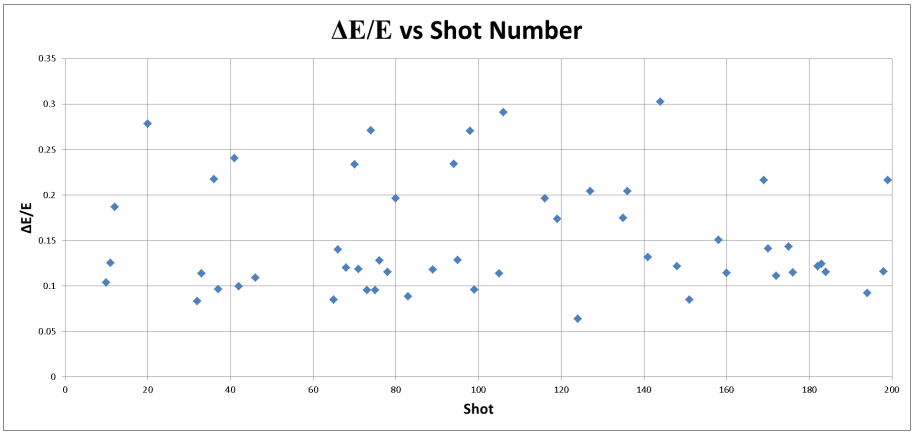

FIGURE 3.6: ΔE/E vs shot number

From the graph, objectively there does not seem to be much of a trend. To verify this, as with the energies before, averages were taken every 5 shots, and error bars added representing the standard deviation of each value making up a point, producing the following graph.

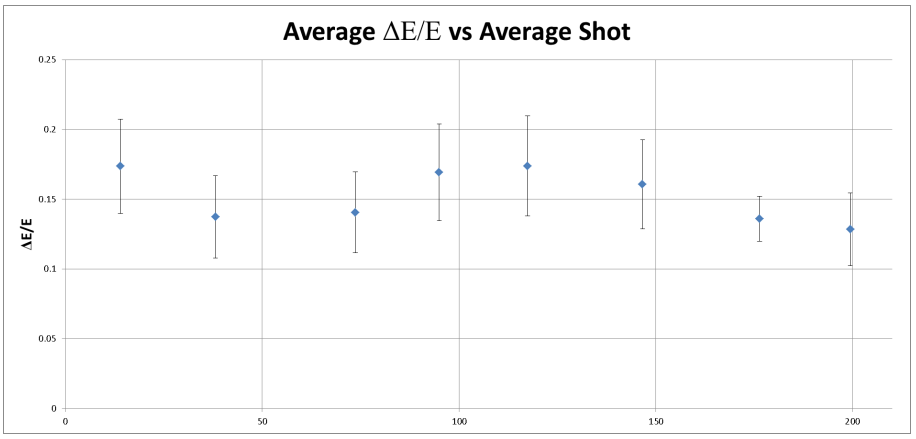

FIGURE 3.7: Average ΔE/E vs shot number, showing error bars

From the above graph, it can be seen that there is no significant trend at all in the data. Thus, the relative widths of the monoenergetic peaks do not change over time as a density gradient is introduced, instead maintaining an average ΔE/E of 0.15, or an FWHM peak width of 15% the peak's maximum energy.

3.2.3 Divergence of the Electron Beam

Since the magnet spectrometers field only affects the electrons in the horizontal plane, the beams width is not affected. This width can be measured by taking a lineout relative brightness in imageJ and calculating the FWHM of the approximately Gaussian profile produced using the MATLAB script mentioned earlier.This will give the width of the electron beam in pixels, which is then converted to length in mm, knowing that 65 pixels is roughly 10mm. Using the values for FWHM and the distance from source to detector (1.3m), equation 2.2 can then be used to calculate the divergence of the beam, which is usually given in mrad.

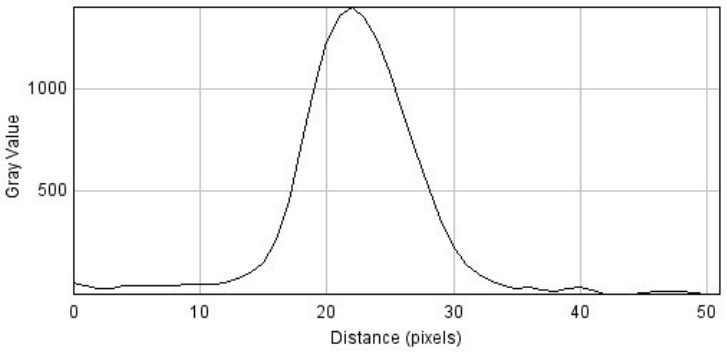

FIGURE 3.8: Example of lineout taken in imageJ of the width of an electron beam, showing the Gaussian profile from which the FWHM can be determined

Note that the width of the beams was calculated at their brightest point, i.e. the divergence of the monoenergetic beams was measured as opposed to the low energy tail. This is because the monoenergetic peaks are the electrons which are relevant to research and applications, whereas the low energy tails are unwanted byproducts of the acceleration process and thus do not contribute to the applications discussed for LWFA electrons. These values for divergence were then also plotted against the shot number to test the aspect of the hypothesis which states that divergence should be unaffected by density gradients in the plasma.

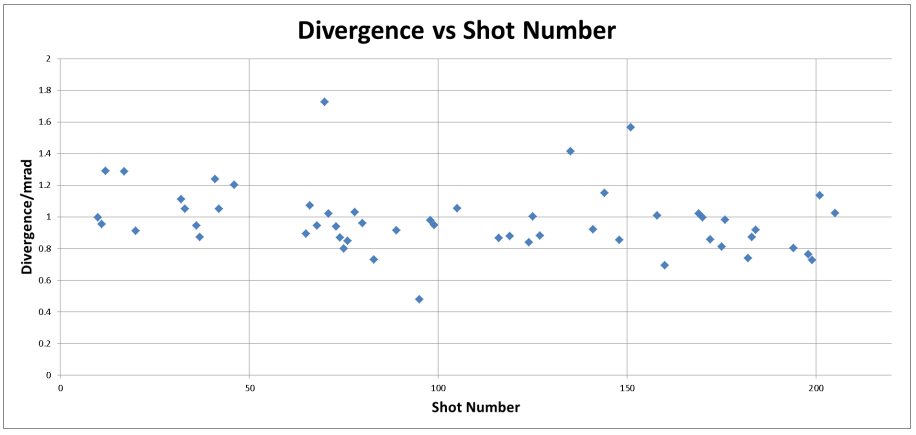

FIGURE 3.9: Divergence of the electron beam in mrad vs shot number

These results show that most beams stay around 1mrad in divergence, meaning that there is no significant trend in the divergence of the beams over time; thus proving the idea that the main factor influencing the divergence of laser wakefield accelerated electron beams is the curvature of the plasma wakefield's wavefronts, and any contribution, if at all, to the divergence from the presence of a density gradient is too small to be significant and so can be considered negligible.

3.2.4 Electron Beam Pointing

The pointing of the electron beam is defined as the relative angle to which the beam deviates from the laser axis and is usually measured in mrad. A stable pointing of the beam is highly important for all applications of electron acceleration, since directions must be precise, for example in Thomson scattering an unstable electron beam pointing directly leads to unstable pointing of the γ-rays for cancer treatment or active interrogation.

To calculate the pointing of the beam, the distance between the beam and the scale present in all images was measured, and an angle calculated in an identical way to how divergence was calculated. This gave an answer in mrad, from which the angular position of the zero point of the laser axis was subtracted to get the true pointing. The

zero point of the laser axis was measured to be 8.6mrad. A graph was produced of the pointing against shot number, as shown in the figure below.

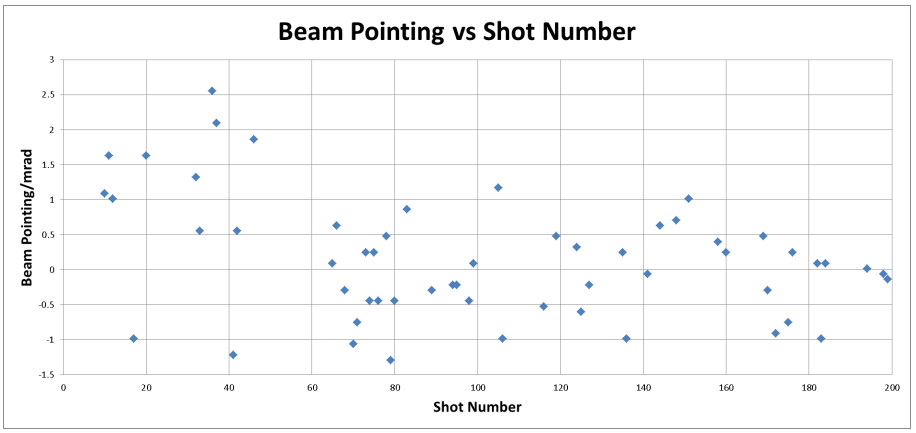

FIGURE 3.10: Beam pointing in mrad vs shot number

As before, the trend is not clear, so averages were once again taken every 5 shots and plotted against the average shot number. Error bars were again calculated as the standard deviation of the points that were averaged.

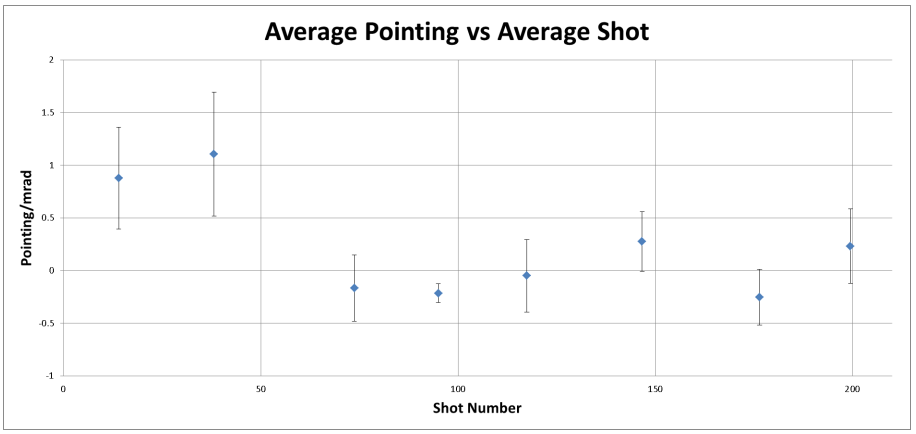

FIGURE 3.11: Average pointing vs average shot number with error bars

It can be seen from the graph above that the pointing is initially unstable on average, eventually stabilising to within less than 0.5mrad of the 0mrad mark after shot ∼70. What this shows is that the density gradient can help stabilise the electron beam, and so utilising this phenomenon could be useful in improving these techniques in the future. However, in order to make the data more reliable, more data points will be needed in future experiments, in conjunction with simulations of LWFA with a density gradient applied to the gas cell to further back up these claims.

Chapter 4

Conclusions

In conclusion, it has been shown that laser wakefield acceleration of electrons is a novel method of production of short bunches of relativistic electrons with applications in many fields of science and industry. There are clear advantages of using ultrashort lasers over LINACs, most notably the much more compact size of the accelerators and shorter electron burst duration, on the order of the laser pulse duration. In addition, the generation of high energy, high brilliance γ-rays via nonlinear Thomson scattering off laser wakefield accelerated electrons offers a much more compact method of high energy photon generation over a standard free electron laser. This radiation has many potential uses in medicine, industry, and security. Further development of the field is needed in order to make these methods commercially viable, as the electron energies can still have poor shot-to-shot stability. However, the techniques are improving as time goes on and soon, table-top sources of stable femtosecond GeV electron bunches or MeV γ pulses will soon be available.

It has been demonstrated that the laser ablation of the gas cell's exit hole introduces an exponentially decaying density gradient that continues on for a distance after the gas cell. This gradient has been shown to accelerate the electrons for a distance longer than the initial gas cell, thus increasing the energy of the beam's monoenergetic peak on average; however the divergence is unaffected by this density gradient as was predicted by the initial hypothesis. The widths of the monoenergetic peaks relative to the peak energy was not seen to change by any significant amount, keeping an FWHM peak width ΔE of 15% the peak's maximum energy for the duration of the experiment. In addition, the pointing of the beam relative to the laser axis was seen to stabilise around the zero point after 70 runs, showing that a density gradient could be used to stabilise beam pointings in the future.

Future experiments would seek to improve on the reliability of the findings presented here by introducing more data points, with the possibility of testing gas cells specifically engineered to produce density gradients of varying degrees. This would help create a quantitative model of the interaction by relating the electron energies to the exit hole diameters. Hydrodynamic and particle-in-cell simulations of the gas leakage and subsequent laser interactions respectively could also be performed in the future with the aim of developing a full working model of the density gradient's effect on laser wakefield acceleration, which currently has only been shown qualitatively.

References

[1] V. Yanovsky, V. Chvykov, G. Kalinchenko, P. Rousseau, T. Planchon, T. Matsuoka, A. Maksimchuk, J. Nees, G. Cheriaux, G. Mourou, and K. Krushelnick. Ultra-high intensity- 300-TW laser at 0.1 Hz repetition rate. *Optical Society of America*, 16: 2109, 2008.

[2] Andrew Weiner. *Ultrafast Optics*. Wiley, 2009.

[3] Orazio Svelto. *Principles of Lasers*. Springer, 5^{th} edition, 2010.

[4] L. Chen, M. Zhang, and Z. Zhang. Dispersion Compensation Devices . In *Frontiers in Guided Wave Optics and Optoelectronics*, chapter 9. InTech, 2010.

[5] Richard Fitzpatrick. *Maxwell's Equations and the Principles of Electromagnetism*. Infinity Science Press, 2008.

[6] T. Tajima and J. M. Dawson. Laser Electron Accelerator. *Physical Review Letters*, 43:267–270, 1979.

[7] Francis F. Chen. *Introduction to Plasma Physics and Controlled Fusion, Volume 1: Plasma Physics*. Springer, 1984.

[8] E.Esarey, C.Schroeder, and W.P.Leemans. Physics of laser-driven plasma-based electron accelerators. *Reviews of Modern Physics*, 81:1229–1285, 2009.

[9] Andrea Macchi. *A Superintense LaserPlasma Interaction Theory Primer*. Springer, 2013.

[10] P. Sprangle and E. Esarey. Interaction of ultrahigh laser fields with beams and plasmas. *Physics of Fluids B: Plasma Physics*, 4(7):2241–2248, 1992.

[11] S. Corde, K. Ta Phuoc, G. Lambert, R. Fitour, V. Malka, A. Rousse, A. Beck, and E. Lefebvre. Femtosecond x rays from laser plasma accelerators. *Reviews of Modern Physics*, 85:1–48, 2013.

[12] J. Faure, Y. Glinec, A. Pukhov, S. Kiselev, S. Gordienko, E. Lefebvre, J.-P. Rousseau, F. Burgy, and V. Malka. A laserplasma accelerator producing monoenergetic electron beams. *Letters to Nature*, 431:541–544, 2004.

[13] W. Lu, M. Tzoufras, C. Joshi, F. S. Tung, W. B. Mori, J. Vieira, R. A. Fonseca, and L. O. Silva. Generating multi-GeV electron bunches using single stage laser wakefield acceleration in a 3D nonlinear regime. *Physical Review ST Accelerators and Beams*, 10:061301, 2007.

[14] S. Gordienko and A. Pukhov. Scalings for ultrarelativistic laser plasmas and quasimonoenergetic electrons. *Physics of Plasmas*, 12(4), 2005.

[15] W.P.Leemans, A. J. Gonsalves, H. S. Mao, K. Nakamura, C. Benedetti, C. B. Schroeder, Cs. Tth, J. Daniels, D. E. Mittelberger, S. S. Bulanov, J. L. Vay, C. G. R. Geddes, and E.Esarey. Multi-GeV Electron Beams from Capillary-Discharge-Guided Subpetawatt Laser Pulses in the Self-Trapping Regime. *Physical Review Letters*, 113:245002, 2014.

[16] F. Mackenroth and A. Di Piazza. Nonlinear Compton scattering in ultrashort laser pulses. *Physical Review A*, 83:032106, 2011.

[17] D. Meyerhofer. High-Intensity-Laser-Electron Scattering. *IEEE Journal of Quantum Electronics*, 33(11):1935–1941, 1997.

[18] K. T. McDonald and K. Shmakov. Classical "Dressing" of a Free Electron in a Plane Electromagnetic Wave. *arXiv:physics/0003059 [physics.acc-ph]*, 2000. URL `http://arxiv.org/abs/physics/0003059`.

[19] G. Sarri, D. J. Corvan, W. Schumaker, J. M. Cole, A. Di Piazza, H. Ahmed, C. Harvey, C. H. Keitel, K. Krushelnick, S. Mangles, Z. Najmudin, D. Symes, A. Thomas, M. Yeung, Z. Zhao, and M. Zepf. Ultrahigh Brilliance Multi-MeV γ-Ray Beams from Nonlinear Relativistic Thomson Scattering. *Physical Review Letters*, 113:224801, 2014.

[20] P. Mayles, A. Nahum, and J.-C. Rosenwald. *Handbook of Radiotherapy Physics - Theory and Practice*. Taylor and Francis, 2007.

[21] G. C. Baldwin and G. S. Klaiber. X-Ray Yield Curves for γ-n Reactions. *Physical Review*, 73:1156–1163, 1948.

[22] American National Standards Institute. American National Standard Minimum Performance Criteria for Active Interrogation Systems Used for Homeland Security. *ANSI N42.41-2007*, 2007.

[23] C.J. Hooker, S. Blake, O. Chekhlov, R.J. Clarke, J.L. Collier, E.J. Divall, K. Ertel, P.S. Foster, S.J. Hawkes, P. Holligan, B. Landowski, W.J. Lester, D. Neely, B. Parry, R. Pattathil, M. Streeter, and B.E. Wyborn. Commissioning the astra gemini petawatt ti:sapphire laser system. pages 1–2, May 2008.

[24] J. Osterhoff, A. Popp, Zs. Major, B. Marx, T. P. Rowlands-Rees, M. Fuchs, M. Geissler, R. Horlein, B. Hidding, S. Becker, E. A. Peralta, U. Schramm, F. Gruner, D. Habs, F. Krausz, S. M. Hooker, and S. Karsch. Generation of Stable, Low-Divergence Electron Beams by Laser-Wakefield Acceleration in a Steady-State-Flow Gas Cell. *Physical Review Letters*, 101:085002, 2008.

[25] D. J. Corvan, G. Sarri, and M. Zepf. Design of a compact spectrometer for high-flux MeV gamma-ray beams. *Review of Scientific Instruments*, 85(6):065119, 2014.

[26] Y.Glinec. *Propagation d'une impulsion laser ultra-intense dans un plasma sous-dense : Génération de faisceaux d'électrons quasi monoénergétiques et développement d'applications.* PhD thesis, Ecole Polytechnique, 2006.